World Academy of Science, Engineering and Technology
International Journal of Energy and Power Engineering
Vol:11, No:4, 2017

Parameters Influencing the Output Precision of a Lens-Lens Beam Generator Solar Concentrator

M. Tawfik, X. Tonnellier, C. Sansom

***Abstract*—**The Lens-Lens Beam Generator (LLBG) is a Fresnel-based optical concentrating technique which provides flexibility in selecting the solar receiver location compared to conventional techniques through generating a powerful concentrated collimated solar beam. In order to achieve that, two successive lenses are used and followed by a flat mirror. Hence the generated beam emerging from the LLBG has a high power flux which impinges on the target receiver, it is important to determine the precision of the system output. In this present work, mathematical investigation of different parameters affecting the precision of the output beam is carried out. These parameters include: Deflection in sun-facing lens and its holding arm, delay in updating the solar tracking system, and the flat mirror surface flatness. Moreover, relationships that describe the power lost due to the effect of each parameter are derived in this study.

***Keywords*—**Fresnel lens, LLBG, solar concentrator, solar tracking.

I. Introduction

INCREASING mankind's population led to growing energy demand. This raised the load on the limited fossil-fuel resources, as they supply nearly 80% of the current world energy requirements [1]. This led to a rapid depletion of such non-renewable energy sources as well as bad environmental impact due to increasing greenhouse gas emissions levels. With a large power availability in sunlight, ranging from about 500 W/m^2 at 60°N latitude to 1000 W/m^2 at the equator measured on a cloudless midsummer's day at noon [2], solar energy represents a reliable, inexhaustible and renewable energy source [3]. Concentrated solar thermal power (CSP) systems, in which direct beam component of solar power is captured [4], can achieve higher conversion efficiencies than photovoltaic systems (PV). Although CSP global market has been expanded with an average rate of 35% per year during a period ranging from 2010 to 2015 [5], more research is required to reduce the cost of CSP systems [6].

Concentrating solar radiation incident on a large aperture area is achieved by reflecting or refracting that flux onto a smaller receiver/absorber area [7]. Typically, reflective solar concentrators are employed in CSP [8]. Linear Fresnel reflectors (LFR) and parabolic troughs (PT) represent the well-known single-axis reflective concentrating systems in which solar radiation is focused onto a focal line where a tube receiver is located [9]-[11]. Although using single-axis tracking in such systems provides an advantage of low structural and operation costs, it cannot allow collecting maximum amount of solar radiation [12]. Accordingly, the limited ability of these systems to track the sun leads to achieving thermal efficiencies ranging from 18% to 59.45% for LFR [13]-[15] and from 21% to71.3% for PT systems [16]-[18]. However, LFR technology has lower capital costs than PT systems despite their lower efficiency range [19], [20]. Furthermore, solar power tower (SPT) and parabolic dish (PD) systems are considered as the renowned forms of dual-axis reflective concentrating systems in which reflected solar radiation is concentrated onto a point where a tube receiver is located [21]-[23]. Dual-axis tracking in such systems provides higher output power compared to single-axis tracking systems [24]. This allows achieving higher efficiencies ranging from 57.3% to 88% for SPT [25]-[27] and from 38% to 80% for PD systems [28]-[30]. On the other hand, refractive-based concentrators use lenses to focus the solar radiation on either a line or point receiver via single or dual-axis tracking mechanisms, respectively [31]-[33]. For linear Fresnel lens (LFL) systems with single-axis tracking, the reported thermal efficiencies vary from 30% to 72.5% [34]-[36]. LFL systems can also be used with dual-axis tracking mechanisms so that a relatively high efficiency ranging from 65% to 69% was achieved [37], [38]. However, theoretical studies dealt with operating LFL with non-tracking mode for reducing costs of such systems [39]-[41]. For the point-focus refractive systems, the maximum theoretical efficiency was found to be 86.8% [42], while the experimental values achieved falls between 27% to 65% [43]-[45].

By the start of 2010s, a point-focus refractive system was introduced by Salem et al. [46], which is called *lens-lens beam generator* (LLBG). The LLBG is a two-stage refractive system in which a concentrated collimated solar beam is generated and directed over a target receiver. It uses a system of two lenses, followed by a flat mirror. An experimental thermal efficiency of 82.65% was achieved on a small scale LLBG prototype [46]. In order to produce large scale LLBG concentrators, further studies need to be carried out. Therefore, it was handled later through investigating some parameters affecting the maximum allowed concentration ratio of the LLBG under different operating conditions [47]. According to this study, high concentration ratios can be

This paper is based upon work funded by the Egyptian Government under the Egyptian Government Full External Missions Funding Program.

Mohamed Tawfik is with Mechanical Power Engineering Department, Faculty of Engineering, Mansoura University, 35516, Egypt. He is a PhD student at Precision Engineering Institute, School of Aerospace, Transport and Manufacturing, Cranfield University, MK43 0AL, UK (corresponding author to provide phone: +44 07774 872759; e-mail: m.m.tawfik@cranfield.ac.uk).

Xavier Tonnellier and Chris Sansom are with Precision Engineering Institute (Global CSP Laboratory), School of Aerospace, Transport and Manufacturing, Cranfield University, MK43 0AL, UK (e-mail: x.p.tonnellier@cranfield.ac.uk, c.l.sansom@cranfield.ac.uk).

achieved by such type of concentrators. Large scale LLBG concentrators with high concentration ratios can generate a powerful beam which may cause damage if impinge off-target area due imprecise estimation of its location over the day-time. However, there are different parameters that may cause shifting or diverging of such generated beam, such as: curvature of the sun-facing lens and deflection of its holding arm, solar tracking system time lag, and the flat mirror surface roughness. These parameters can affect the output beam as well as the total system performance. In the present work, the relationships between such parameters and output precision and system efficiency are mathematically investigated.

II. LLBG Design and Nomenclatures

The LLBG system is consisting of two successive converging lenses. This optical configuration is known as *telecentric lenses* [48]. The *front lens* faces the incident solar radiation and concentrates at its focal point which is coincident with the *rear lens* focus. The two lenses are linked via an arm, called *main arm*, which tracks the sun altitude, α, and azimuth, φ, angles. In order to control the direction of the generated beam over the day-time, a flat mirror, named *control mirror*, is used during the tracking process to direct the generated beam onto the required target. These main parts are illustrated in Fig. 1.

III. Parameters Influencing LLBG Output

In this section, mathematical analysis of different parameters affecting the precision of the LLBG output is carried out. For each parameter a relation with the loss in concentrated power is derived. These parameters include: Main arm deflection, delay in sun tracking, front lens curvature and control mirror surface flatness.

A. Front Lens Buckling

Building a large scale LLBG requires using a front lens with a large area. Fresnel lenses are typically employed for applications that require large aperture areas [49]. Plastic is commonly used in fabricating such non-imaging Fresnel optics [50]. Gravity, wind-load, thermal- or hydro-expansion, and shrinkage can cause lens buckling [51]. Lens buckling was found to shift its focal point [52]–[54].

In order to study the effect of the large Fresnel lens bending, rays can be traced at one prism of the lens which lies at a distance, r, from the lens centerline. The incident ray is assumed to be parallel with the lens major axis with an incidence angle, θ_1, with the prism surface. The prism deflects the ray to exit the lens with an angle of refraction, θ_2, to be directed to the focal point, as shown in Fig. 2.

Fig. 2 illustrates incidence and refraction angles of rays at a certain prism in normal condition. Assuming lens in Fig. 2 has been deflected with a radius of curvature, R_C, and then the studied prism will rotate by an angle of $d\theta$, as shown in Fig. 3.

Based on geometry of Fig. 3, it seems to be analogous to *spherical aberration* geometry shown in Fig. 4. Spherical aberration is produced by rotationally symmetrical surfaces centered and orthogonal in regard to the optical axis [55]. In that aberration paraxial rays, denoted by P in Fig. 4, are focused at a point P' while curvature, R_C, of the lens surface at the marginal rays, denoted by M in Fig. 4, are focused at a point M'. The distance between P' and M', denoted by LA in Fig. 4, represents *longitudinal aberration*.

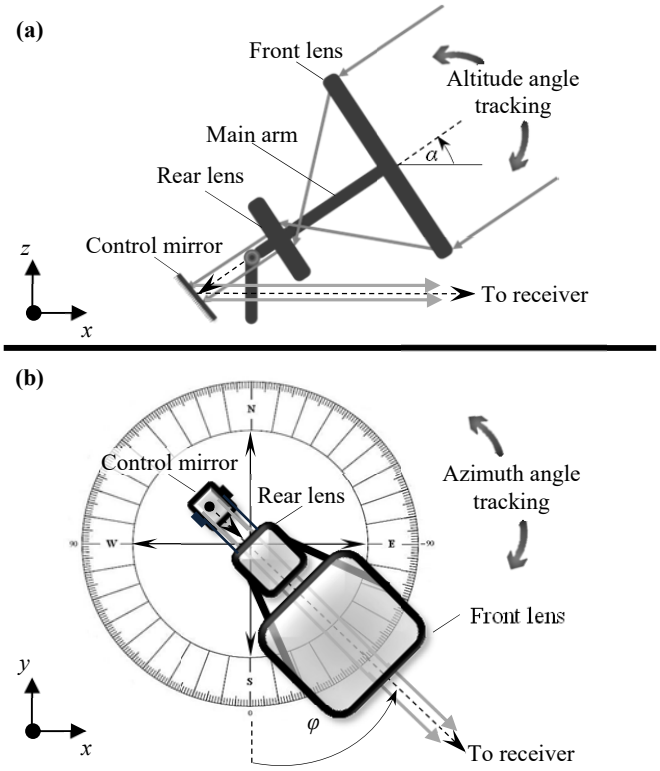

Fig. 1 LLBG nomenclatures (a) Side view (x-z plan), (b) Top view (x-y plan)

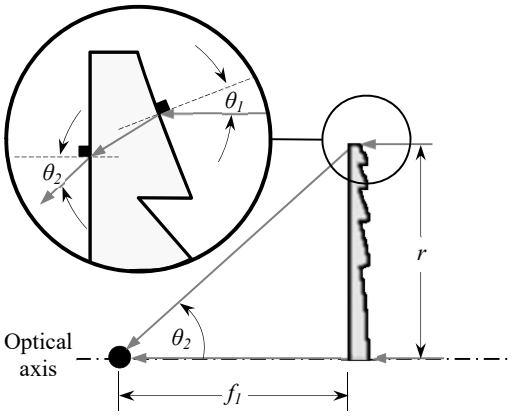

Fig. 2 Incidence and refraction angles on a Fresnel lens prism

The analogy between Figs. 3 and 4 arises from changing of the incidence angle by $d\theta$ in case of Fig. 3 which corresponds the angle Δ in Fig. 4. Therefore, the same effect of changing the focal point location is achieved. Table I lists and describes the analogous main parameters between Figs. 3 and 4.

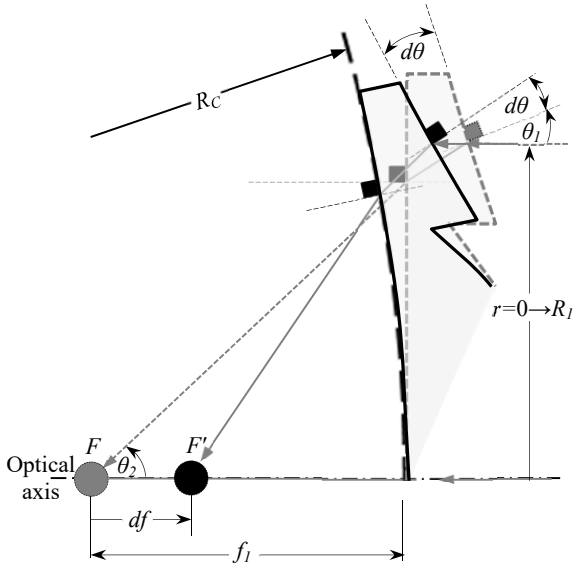

Fig. 3 Geometry of a prim in a bended Fresnel lens

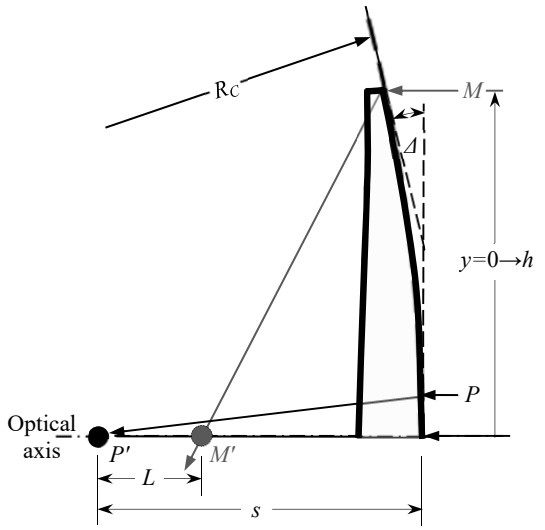

Fig. 4 Geometry describing spherical aberration [56]

TABLE I
ANALOGY BETWEEN BENDED FRESNEL AND SPHERICAL ABERRATION

Bended Fresnel Lens (Fig. 3)		Spherical Aberration (Fig. 4)	
Symbol	Description	Symbol	Description
R_C	Radius of curvature	R_C	Radius of curvature
r	Distance from optical axis	y	Distance from optical axis
R_1	Fresnel lens radius (width)	h	Lens radius
f_1	Focal length (unbent)	s	Paraxial focal length
F	Fresnel lens focus	P'	Paraxial focus
F'	Shifted focus (bent lens)	M'	Marginal focus
df	Focus position deviation	LA	Longitudinal aberration
$d\theta$	Change in incidence angle	Δ	Change in incidence angle

Applying the *third order theory* to a case similar to Fig. 4, then the spherical aberration can be determined from [57]:

$$\left|LA\right|_{y=h} = s^2\left(da/dy\right)/\left(n.y\right) \tag{1}$$

where n is the refractive index of the lens material and a is *wave aberration* function and (da/dy) is the local curvature which can be expressed as [57]:

$$da\,/\,dy = n\Delta \tag{2}$$

where from geometry of Fig. 4:

$$\Delta = \sin^{-1}\left(h\,/\,R_C\right) \tag{3}$$

By substitution in (1) at (y=h), then spherical aberration can be determined from:

$$\left|LA\right| = s^2\Delta/h \tag{4}$$

Using analogy between spherical aberration and focal length deviation, then equation (4) can be re-written in terms of bent Fresnel lens case (Fig. 3) as follows:

$$\left|df\right| = f_1^2\left(d\theta\right)/R_1 \qquad \text{and} \qquad d\theta = \sin^{-1}\left(R_1\,/\,R_C\right) \tag{5}$$

However, direction of focal point deviation depends on the bending form of the front lens, as illustrated in Fig. 5. Convex- and concave-shape bending of the front lens shifts the focal point before or after the original focal point F generating a pre- or post-focus, respectively.

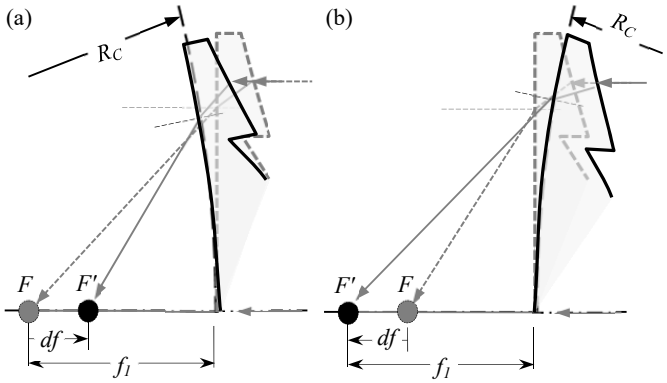

Fig. 5 Focal point shifting (a) Convex bending (pre-focus), (b) Concave bending (post-focus)

In order to determine the effect of front lens buckling on the power lost form the generated beam, the combination with the rear lens is required to be studied. Thick rear lens will absorb much power of concentrated, leading to reduction in optical efficiency and reaching rear lens critical temperature [47]. Therefore, it is recommended to use thin rear lens. Based on that, assumption of using thin rear lens will be considered in the ray tracing process, which is illustrated in Fig. 6. The thin lens equation can be expressed as [58]:

$$f_2^{-1} = s_1^{-1} + s_2^{-1} \tag{6}$$

Hence the aim is to determine the distance s2, the previous equation can be written in the following form:

(7)

$$s_2 = (f_2.s_1)/(s_1 - f_2)$$

From the geometry of Fig. 6:

$$s_2 = (f_2.df \pm f_2^2)/df \quad (8)$$

where the (+) is for pre-focus case, while (–) is for the post-focus case.

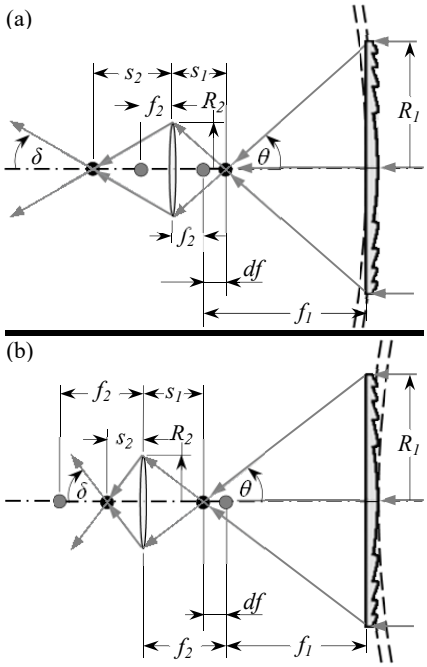

Fig. 6 Front-Rear lenses configuration with bent front lens
(a) Convex bending (pre-focus), (b) Concave bending (post-focus)

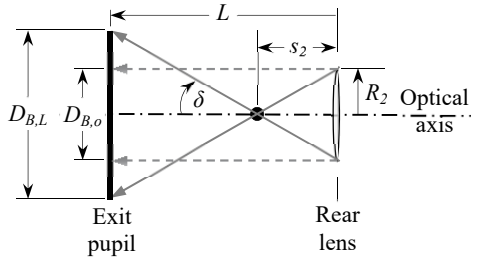

Fig. 7 Beam divergence

In order to determine the amount of lost power from the generated beam, it is essential to determine the beam deviation angle, δ, which can be determined as:

$$\delta = \tan^{-1}(R_2/s_2) \quad (9)$$

From (8) in (9) then:

$$\delta = \tan^{-1}\left((R_2.df)/(f_2.df \pm f_2^2)\right) \quad (10)$$

In the last equation, when ($df \rightarrow 0$), then ($\delta \rightarrow 0$) which means that precise focusing from the front lens leads to minimum beam deviation. Equation (10) also shows that post-focus case, in which the front lens is buckled in a concave form, boosts the beam deviation of the generated beam compared to the pre-focus case.

Based on deviation angle calculated from (10) the original beam diameter $D_{B,o}$ will increased to $D_{B,L}$ after travelling a distance L, as illustrated in Fig. 7.

From geometry of Fig. 7, the original beam diameter, $D_{B,o}$, can be determined from:

$$D_{B,o} = 2R_2 \quad (11)$$

The diverged beam diameter, $D_{B,L}$, at distance L from the rear lens center can be calculated from:

$$D_{B,L} = 2|L - s_2|\tan\delta \quad (12)$$

Then the beam diameter ratio is:

$$D_{B,L}/D_{B,o} = \left(|L - s_2|\tan\delta\right)/R_2 \quad (13)$$

Hence the power collected is a function of beam area, then the power loss due to lens buckling, PL_b, can be determined as:

$$PL_b = (D_{B,L}/D_{B,o})^2 - 1 \quad \text{(for } D_{B,L} > D_{B,o}\text{)} \quad (14.a)$$

$$PL_b = 0 \quad \text{(for } D_{B,L} \le D_{B,o}\text{)} \quad (14.b)$$

Or it can be rewritten as follows:

$$PL_b(L, f_1, R_1, f_2, R_2, R_C) = \left[\left(|L - s_2|\tan\delta\right)/R_2\right]^2 - 1 \quad \text{(for } D_{B,L} > D_{B,o}\text{)} \quad (15.a)$$

$$PL_b(L, f_1, R_1, f_2, R_2, R_C) = 0 \quad \text{(for } D_{B,L} \le D_{B,o}\text{)} \quad (15.b)$$

Input parameters of (15) can be determined from (5), (8) and (10).

B. Main Arm Deflection

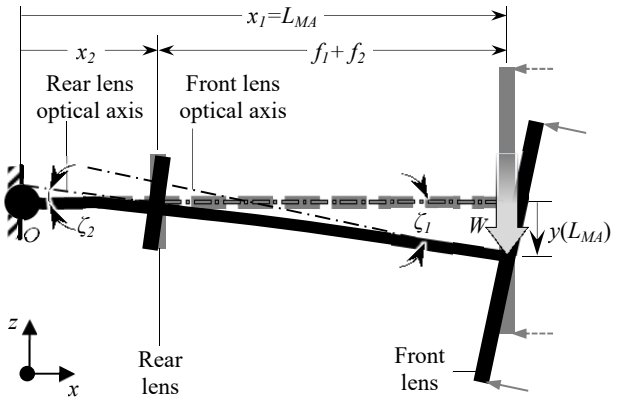

Fig. 8 Main arm deflection

The main arm and the front lens weights represent major sources of its deflection. If point O is the axis of rotation, the main arm with a total length of L_{ma} can be considered as a cantilever fixed at point O and subjected to a total weight

force, W, at its end, as illustrated in Fig. 8.

Assuming the cantilever deflection case due to force, W, acting at L_{MA}, then the general form of deflection, y, at any distance, x, measured from the point O can be described by [59]:

$$y(x) = \left(W\left(x^3 - 3L_{MA}x^2\right)\right)/(6EI) \tag{16}$$

where E is the modulus of elasticity and I is the moment of inertia. According to Fig. 8 geometry, deflection tilts the optical axes of both front and rear lenses by angles ζ_1 and ζ_2, respectively. These angles can be determined from:

$$\tan\zeta_1 = \left(dy/dx\right)_{x=L_{MA}} = \left(-WL_{MA}^2\right)/(2EI) \tag{17}$$

$$\tan\zeta_2 = \left(dy/dx\right)_{x=x_2} = \left(W\left(x_2^2 - 2L_{MA}x_2\right)\right)/(2EI) \tag{18}$$

Then, a relative position between the front and rear optical axes can be considered, as illustrated in Fig. 9. For that position, the relative angle between front and rear lenses optical axes, ζ, can be expressed as:

$$\zeta = \zeta_1 - \zeta_2 = \tan^{-1}\left(\left(-WL_{MA}^2\right)/(2EI)\right) - \tan^{-1}\left(\left(W\left(x_2^2 - 2L_{MA}x_2\right)\right)/(2EI)\right) \tag{19}$$

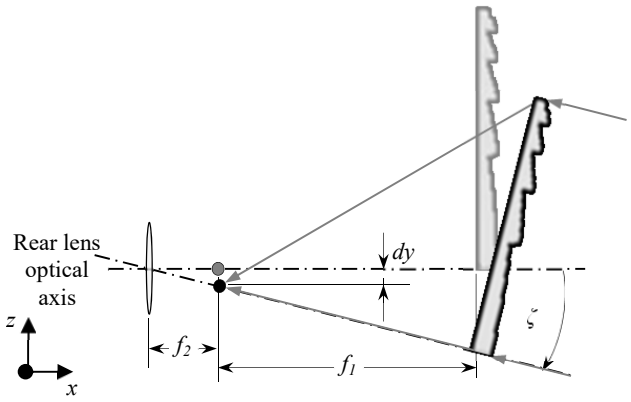

Fig. 9 Relative position between front and rear lenses optical axes

Assuming that the ideal dual axis tracking system is in use, then mechanical deflection of the main arm, due to the front lens and its own weight, by a relative angle ζ shifts the front lens's focal point by dy, is shown in Fig. 9.

The shifted focal point can be considered as a light source at an off-axis secondary focal point of the rear lens. This will lead to generate a beam with rays parallel to each other, but not necessarily to the rear lens optical axis [60]. Assuming that the front lens optical axis passes through the rear lens center, then:

$$dy = f_2 \tan\zeta \tag{20}$$

When rays emerging from the shifted focal point are encountered by the rear lens, a tilted beam with an angle ζ can be generated at the leaving surface of rear lens [61], as illustrated in Fig. 10.

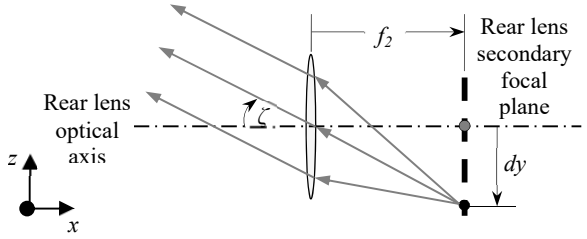

Fig. 10 Off-axis light source at a secondary focal point [60], [61]

In order to determine the amount of power lost due to main arm deflection, PL_{MA} at a distance, L, from the rear lens center, geometry in Fig. 11 can be considered.

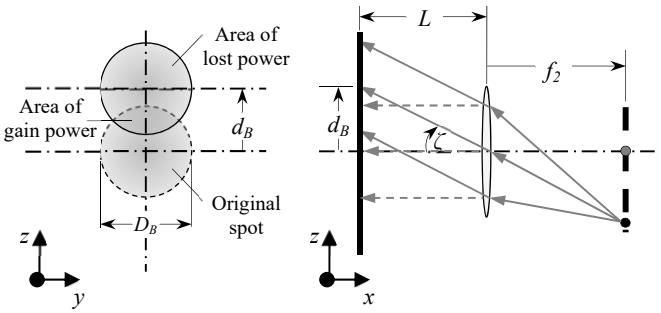

Fig. 11 Shifted beam and lost power

From geometry, main arm deflection leads to shifting the generated spot by d_B, which can be determined from:

$$d_B = \left|L\tan(\zeta)\right| \tag{21}$$

Hence the power collected from input solar flux is directly proportional to the surface area, the beam area can be used as an indication of amount gained or lost from collected power. Assuming the shifted beam is circular with diameter, D_B, then the gain area of the beam, A_g, which is the intersection area between the two circles of original and shifted beams, can be determined as follows [62]:

$$A_g = 0.5\left[\begin{matrix}\left(D_B^2\cos^{-1}\left(d_B/D_B\right)\right) \\ -d_B\sqrt{\left(D_B + d_B\right)\left(D_B - d_B\right)}\end{matrix}\right] \tag{22}$$

Then the area of lost power, A_L, can be determined from:

$$A_L = A_o - A_g \tag{23}$$

where, A_o is the original beam surface area. Then, the lost power is PL_{MA}:

$$PL_{MA} = 1 - \left(A_g/A_o\right) \tag{24}$$

Or

$$PL_{MA}(L,D_B,L_{MA},E,I)=1-\begin{bmatrix}(2/\pi)\cos^{-1}(d_B/D_B)\\-(2d_B/\pi D_B^2)*\\\sqrt{(D_B+d_B)(D_B-d_B)}\end{bmatrix}$$

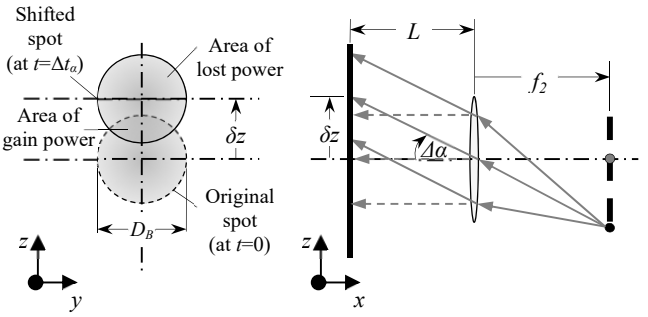

Fig. 12 Altitude angle error

C. Delay in Tracking System

There are two major methods to track the sun: time-based and sensor-based methods [63]. The time-based method, which is also known as the astronomical method, acts as an open-loop control system [64]. In such sensorless technique, data obtained from different sun path charts or solar angles equations are used to identify and follow the sun position [65]. The sensor-based, which is known as the optical method, acts as a closed-loop control system in which several feedback sensors are used to track the sun [66]. The time-based method is much simpler and cheaper compared to the sensor-based method [67]. Moreover, time-based method is less sensitive to weather conditions [63]. However, tracking accuracy cannot be guaranteed in case of employing time-based method as a result of installation and the time errors [68]. Therefore, minimizing tracking errors requires using a hybrid strategy combining both methods [63]. Many researchers have been concerned with evaluating the tracking error of their systems [63], [64], [66], [69]-[71]. In this section, a mathematical study is carried out to evaluate the tracking error effect on LLBG performance. This evaluation can be used in defining the accepted tolerance and suitable tracking method in carried out designs. Hence, the LLBG requires a dual-axis tracking, errors in both altitude and azimuth angles require investigation. In both cases, delay in control system interaction with its input data, i.e. time or feedback sensors signals, inclines the incident solar rays with respect to the front lens optical axis. This delay can be divided into two major ones: (1) Δt_α, which represents the time interval delay in tracking the altitude angle, α, (2) Δt_φ, which represents the delay in tracking the azimuth angle, φ. Both leads to converging the rays at an off-axis secondary focal point of the rear lens [60]. When rays emerging from that secondary focal point come across the rear lens, a tilted beam with an angle can be generated at the leaving surface of rear lens [61]. This case seems to be similar to the case discussed before in section B. In the following subsections, analogy with deflected main arm's case will be applied to evaluate the effect of tracking error in both altitude and azimuth angles.

1) Altitude Angle Error

When the control system is delayed by a time interval Δt_α, the altitude angle, α, will be changed with an angle $\Delta\alpha$. This means that the rays from the shifted focal point will leave the rear lens surface with an angle $\Delta\alpha$ which shifts the generated beam with, δz, as illustrated in Fig. 12.

From geometry of Fig. 12, the amount of spot shift at a distance L from the rear lens center can be determined by:

$$\delta z = L\tan(\Delta\alpha) \tag{25}$$

Then, the amount of power lost due to altitude angle tracking error, PL_α at a distance, L, from the rear lens center can be evaluated as:

$$PL_\alpha(L,D_B,\Delta t_\alpha)=1-\begin{bmatrix}(2/\pi)\cos^{-1}(\delta z/D_B)\\-(2\delta z/\pi D_B^2)*\\\sqrt{(D_B+\delta z)(D_B-\delta z)}\end{bmatrix} \tag{26}$$

2) *Azimuth Angle Error*

Delaying the control system by a time interval Δt_φ, leads to changing the azimuth angle, φ, with an angle $\Delta\varphi$. This means that the emerged rays from the shifted focal point will make an angle $\Delta\varphi$ with the optical axis of the rear lens. This shifts the generated beam with, δy, as illustrated in Fig. 13.

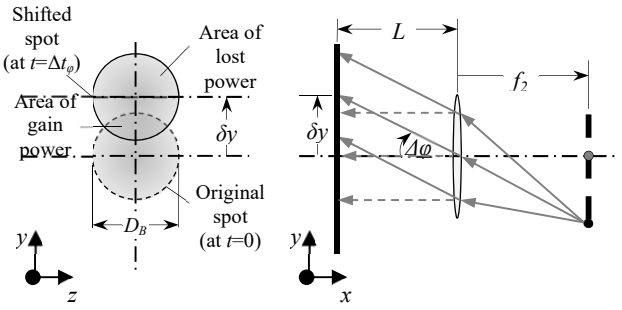

Fig. 13 Azimuth angle error

From geometry of Fig. 13, the amount of spot shift at a distance L from the rear lens center can be determined by:

$$\delta y = L\tan(\Delta\varphi) \tag{27}$$

Then, the amount of power lost due to azimuth angle tracking error, PL_φ at a distance, L, from the rear lens center can be evaluated as:

$$PL_\varphi(L,D_B,\Delta t_\varphi)=1-\begin{bmatrix}(2/\pi)\cos^{-1}(\delta y/D_B)\\-(2\delta y/\pi D_B^2)*\\\sqrt{(D_B+\delta y)(D_B-\delta y)}\end{bmatrix} \tag{28}$$

D. Control Mirror Flatness

Mirror flatness/roughness is used as a measure of mirror surface deviation from a perfectly flat surface [72]. Mirror surface roughness scatters the incident light. The diffused scattering increases with roughness increase. For slight rough

surfaces, the reflected light is diffused in the specular direction. As roughness increases, the reflected light is diffused in more directions until a uniform scattering in all directions occurs at the case with maximum roughness, as illustrated in Fig. 14 [73], [74]. The diffused light represents power loss.

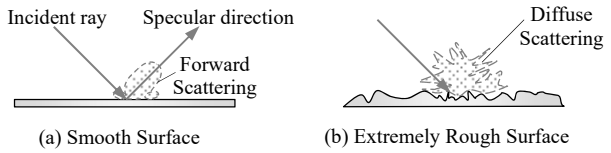

Fig. 14 Light scattering from: (a) smooth surface (b) extremely rough surface

Mirror surface roughness can be defined as the absolute difference between the highest (peaks) and lowest points (valleys) on the mirror surface [75]. Such deviation is typically measured in fractions of a wavelength of 632.8 nm light per inch of optical surface. Mirror surface roughness can also be expressed in terms of the root mean square (RMS) flatness, in which the standard deviation of the optical surface from the ideal surface is calculated [76]. The difference between both methods is illustrated in Fig. 15.

Fig. 15 Peaks to Valleys vs RMS flatness expressing methods

In order to determine the power loss due to mirror surface roughness, it is important to calculate the diffusely scattered portion of the incident light. It can be expressed in terms of total integrated scattering (TIS), which is defined as the ratio between the diffusely scattered radiant power by the surface (diffuse reflectance) and the total reflected power (specular plus diffuse reflectance [77]:

$$\text{TIS} = \text{Diffused reflectance} / \text{Total reflectance} \quad (29)$$

By applying the scalar scattering theory, which is based on the Kirchhoff diffraction integral, the TIS and the amount of power lost due to mirror surface roughness, PL_{sr}, can be determined as [77]–[80]:

$$PL_{sr} = TIS = 1 - \exp[-(4\pi * RMS \cos\theta_i / \lambda)^2] \quad (30)$$

where, RMS is the root mean square of surface roughness in (nm), θ_i is the incidence angle and λ is wavelength of the incident radiation in (nm). However, commercial specifications of mirror surface roughness are usually expressed in terms of the absolute difference between peaks and valleys which is known as total roughness, R_t. In such cases, there are tables to convert surface roughness between such industrial expressions. Data available to convert R_t into RMS are plotted in Fig. 16 [81]. The plotted data were found to conform to a 4th order polynomial fit with:

$$RMS = (8\text{E-}14)R_t^4 - (1\text{E-}09)R_t^3 + (5\text{E-}06)R_t^2 + (0.1353)R_t - 6.7311 \quad (31)$$

Equation (31) can be used to get an approximate value of RMS to be applied in (30).

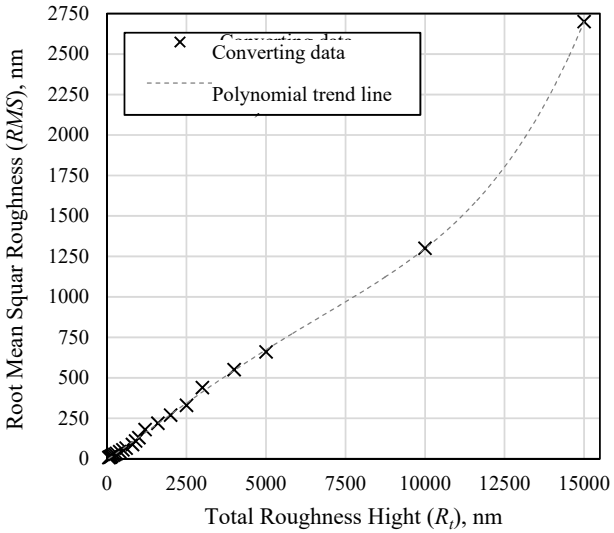

Fig. 16 Converting total roughness (R_t) into RMS [81]

IV. Conclusion

The LLBG is a Fresnel-based configuration which can generate a concentrated beam of solar radiation. It employs two-stage refracting optical system followed by a flat mirror. The present study investigated mathematically different parameters influencing the output beam precision and power lost due to each parameter. These parameters included: front lens buckling, deflection of the main arm, solar tracking system delay, and the flat mirror surface roughness.

For the deflection in the front lens, it is found to be responsible of shifting its actual focal backwards or forward depending on the radius of curvature of the bended lens. Both of holding arm deflection and delay in updating the solar tracking system were found to shift the generated beam away from its target area according to the amount of deflection/delay and the length between the LLBG and the target plan. The mirror surface flatness is found to be affecting the amount of scattered reflected light. The more roughness, the more power lost due diffusive scattering on the mirror surface.

References

[1] A. Kumar, "Improvements in efficiency of solar parabolic trough," *IOSR J. Mech. Civ. Eng.*, vol. 7, no. 6, pp. 63–75, 2013.
[2] J. Houghton, *Global Warming: The Complete Briefing*, 3rd Ed. Cambridge University Press, 2004.
[3] L. R. Wilson, "Luminescent Solar Concentrators : A Study of Optical Properties, and Device Optimisation," Heriot-Watt University, 2010.
[4] R. Österholm and J. Pålsson, "Dynamic modelling of a parabolic trough solar power plant," in *Proceedings of the 10th International Modelica Conference*, 2014, p. 1057.
[5] REN21, "Renewables 2016 Global Status Report," Paris, 2016.
[6] R. Pitchumani, "SunShot Initiative," Washington D.C., USA, 2014.
[7] C. C. Newton, "A Concentrated Solar Thermal Energy System," Florida

State University, 2007.
[8] M. Mancini, T., Kolb, G., and Prairie, "Solar Thermal Power," in *Advances in Solar Energy: An Annual Review of Research and Development*, Volume 11, K. W. Böer, Ed. Boulder, CO: American Solar Energy Society, 1997, pp. 1–42.
[9] S. A. Kalogirou, *Solar Energy Engineering*. Elsevier, 2009.
[10] M. Günther, M. Joemann, and S. Csambor, "Parabolic Trough Technology," in *Advanced CSP Teaching Materials*, Kassel, Germany: Enermena; German Aerospace Center (DLR), 2011.
[11] D. R. Mills, "Linear Fresnel reflector (LFR) technology," in *Concentrating Solar Power Technology: Principles, Developments and Applications*, K. Lovegrove and W. Stein, Eds. Cambridge, UK: Woodhead Publishing Limited, 2012, pp. 153–196.
[12] C. Chang, "Tracking solar collection technologies for solar heating and cooling systems," in *Advances in Solar Heating and Cooling*, R. Wang and T. Ge, Eds. Woodhead Publishing Limited, 2016, pp. 81–93.
[13] S. Gianella, "Porous Materials for High-Temperature Solar Absorbers," in *International Symposium on High Temperature Solar Materials*, 2012.
[14] S. A. Kalogirou, "Solar Thermal Power Systems," in *Solar Energy Engineering - Processes and Systems*, 2nd Ed., Elsevier, 2014, pp. 541–581.
[15] G. Cau and D. Cocco, "Comparison of Medium-size Concentrating Solar Power Plants based on Parabolic Trough and Linear Fresnel Collectors," *Energy Procedia*, vol. 45, pp. 101–110, 2014.
[16] M. Eck and E. Zarza, "Saturated steam process with direct steam generating parabolic troughs," *Sol. Energy*, vol. 80, no. 11, pp. 1424–1433, Nov. 2006.
[17] N. El Gharbi, H. Derbal, S. Bouaichaoui, and N. Said, "A comparative study between parabolic trough collector and linear Fresnel reflector technologies," *Energy Procedia*, vol. 6, pp. 565–572, 2011.
[18] A. Rovira, R. Barbero, M. J. Montes, R. Abbas, and F. Varela, "Analysis and comparison of Integrated Solar Combined Cycles using parabolic troughs and linear Fresnel reflectors as concentrating systems," *Appl. Energy*, vol. 162, pp. 990–1000, 2016.
[19] G. Morin, J. Dersch, W. Platzer, M. Eck, and A. Häberle, "Comparison of Linear Fresnel and Parabolic Trough Collector power plants," *Sol. Energy*, vol. 86, no. 1, pp. 1–12, Jan. 2012.
[20] IRENA, "Renewable Power Generation Costs in 2012 : An Overview," 2013.
[21] C. L. Martin and D. Y. Goswami, *Solar Energy Pocket Reference*. Routledge, 2005.
[22] B. Sørensen, P. Breeze, T. Storvick, S.-T. Yang, A. V. da Rosa, H. K. Gupta, R. Sukanta, M. Doble, P. Maegaard, G. Pistoia, and S. Kalogirou, *Renewable Energy Focus Handbook*, 1st Ed. Academic Press, 2009.
[23] J. P. Kesari, M. Gupta, A. Jain, and A. K. Ojha, "Review of the Concentrated Solar Thermal Technologies : Challenges and Opportunities in India," *Int. J. Res. Sci. Innov.*, vol. II, no. I, pp. 105–111, 2015.
[24] Dhanabal R, B. V, Ranjitha R, Ponni A, D. S, and Mageshkannan P, "Comparison of Efficiencies of Solar Tracker systems with static panel Single- Axis Tracking System and Dual-Axis Tracking System with Fixed Mount," *Int. J. Eng. Technol.*, vol. 5, no. 2, pp. 1925–1933, 2013.
[25] G. Franchini, A. Perdichizzi, S. Ravelli, and G. Barigozzi, "A comparative study between parabolic trough and solar tower technologies in Solar Rankine Cycle and Integrated Solar Combined Cycle plants," *Sol. Energy*, vol. 98, pp. 302–314, Dec. 2013.
[26] J. E. Pacheco, H. E. Reilly, G. J. Kolb, and C. E. Tyner, "Summary of the Solar Two: Test and Evaluation Program," 2000.
[27] F. J. Collado, "Quick evaluation of the annual heliostat field efficiency," *Sol. Energy*, vol. 82, no. 4, pp. 379–384, Apr. 2008.
[28] J.-L. Bouvier, G. Michaux, P. Salagnac, T. Kientz, and D. Rochier, "Experimental study of a micro combined heat and power system with a solar parabolic trough collector coupled to a steam Rankine cycle expander," *Sol. Energy*, vol. 134, pp. 180–192, Sep. 2016.
[29] Y. Rafeeu and M. Z. A. Ab Kadir, "Thermal performance of parabolic concentrators under Malaysian environment: A case study," *Renew. Sustain. Energy Rev.*, vol. 16, no. 6, pp. 3826–3835, Aug. 2012.
[30] N. Kaushika and K. Reddy, "Performance of a low cost solar paraboloidal dish steam generating system," *Energy Convers. Manag.*, vol. 41, no. 7, pp. 713–726, 2000.
[31] D. T. Nelson, D. L. Evans, and R. K. Bansal, "Linear Fresnel lens concentrators," *Sol. Energy*, vol. 17, no. 5, pp. 285–289, Nov. 1975.
[32] G. Wang, Z. Chen, P. Hu, and X. Cheng, "Design and optical analysis of the band-focus Fresnel lens solar concentrator," *Appl. Therm. Eng.*, vol. 102, pp. 695–700, Jun. 2016.
[33] S. R. Kurtz, "Opportunities and challenges for development of a mature concentrating photovoltaic power industry," 2012.
[34] M. Lin, K. Sumathy, Y. J. Dai, and X. K. Zhao, "Performance investigation on a linear Fresnel lens solar collector using cavity receiver," *Sol. Energy*, vol. 107, pp. 50–62, Sep. 2014.
[35] H. Zhai, Y. J. Dai, J. Y. Wu, R. Z. Wang, and L. Y. Zhang, "Experimental investigation and analysis on a concentrating solar collector using linear Fresnel lens," *Energy Convers. Manag.*, vol. 51, no. 1, pp. 48–55, Jan. 2010.
[36] I. Soriga and C. Neaga, "Thermal analysis of a linear Fresnel lens solar collector with black body cavity receiver," *UPB Sci. Bull. Ser. D Mech. Eng.*, vol. 74, no. 4, pp. 105–116, 2012.
[37] K. E. J. Al-Jumaily and M. K. A. Al-Kaysi, "The study of the performance and efficiency of flat linear Fresnel lens collector with sun tracking system in Iraq," *Renew. Energy*, vol. 14, no. 1–4, pp. 41–48, May 1998.
[38] F. Franc, V. Jirka, M. Malý, and B. Nábělek, "Concentrating collectors with flat linear fresnel lenses," *Sol. Wind Technol.*, vol. 3, no. 2, pp. 77–84, Jan. 1986.
[39] R. Leutz, A. Suzuki, A. Akisawa, and T. Kashiwagi, "Design of a nonimaging Fresnel lens for solar concentrators," *Sol. Energy*, vol. 65, no. 6, pp. 379–387, Apr. 1999.
[40] R. Leutz, A. Suzuki, A. Akisawa, and T. Kashiwagi, "Shaped nonimaging Fresnel lenses," *J. Opt. A Pure Appl. Opt.*, vol. 2, no. 2, pp. 112–116, Mar. 2000.
[41] R. Leutz, A. Suzuki, A. Akisawa, and T. Kashiwagi, "Nonimaging Fresnel Lenses of Low and Medium Concentration for Cost-Effective Photovoltaic Systems," in *World Renewable Energy Congress VI*, Elsevier, 2000, pp. 832–835.
[42] V. M. Andreev, A. S. Vlasov, V. P. Khvostikov, O. A. Khvostikova, P. Y. Gazaryan, S. V. Sorokina, and N. A. Sadchikov, "Solar Thermophotovoltaic Converters Based on Tungsten Emitters," *J. Sol. Energy Eng.*, vol. 129, no. 3, pp. 298–303, 2007.
[43] V. M. Andreev, A. S. Vlasov, V. P. Khvostikov, O. A. Khvostikova, P. Y. Gazaryan, N. A. Sadchikov, and V. D. Rumyantsev, "Solar Thermophotovoltaic Converter with Fresnel Lens and GaSb Cells," in *2006 IEEE 4th World Conference on Photovoltaic Energy Conference*, 2006, vol. 1, pp. 644–647.
[44] W. Xie, Y. Dai, and R. Wang, "Numerical and experimental analysis of a point focus solar collector using high concentration imaging PMMA Fresnel lens," *Energy Convers. Manag.*, vol. 52, no. 6, pp. 2417–2426, Jun. 2011.
[45] W. Xie, Y. Dai, and R. Wang, "Theoretical and experimental analysis on efficiency factors and heat removal factors of Fresnel lens solar collector using different cavity receivers," *Sol. Energy*, vol. 86, no. 9, pp. 2458–2471, Sep. 2012.
[46] M. S. Salem, M. Tawfik, and A. Hamed, "Analysis and Performance of Solar Concentrating-Tracking System," in *7th General International Engineering Conference*, 2010.
[47] M. M. Tawfik and M. S. Salem, "Key parameters affecting concentration ratio of a solar concentrator based on lens-lens beam generator configuration," in *43rd ASES National Solar Conference 2014, SOLAR 2014*, 2014, vol. 1.
[48] M. Watanabe and S. K. Nayar, "Telecentric Optics for Focus Analysis," *IEEE Trans. Pattern Anal. Mach. Intell.*, vol. 19, no. 12, pp. 1360–1365, 1997.
[49] N. Enteria and A. Akbarzadeh, *Solar Energy Sciences and Engineering Applications*. Leiden, The Netherlands: CRC Press, 2013.
[50] S. Bäumer, *Handbook of Plastic Optics*, 2nd Ed. Wiley VCH, 2010.
[51] D. C. Miller and S. R. Kurtz, "Durability of Fresnel lenses: A review specific to the concentrating photovoltaic application," *Sol. Energy Mater. Sol. Cells*, vol. 95, no. 8, pp. 2037–2068, Aug. 2011.
[52] P. Rai-Choudhury, *Handbook of Microlithography, Micromachining, and Microfabrication, Volume 2: Micromachining and Microfabrication*. Washington D.C., USA: SPIE, 1997.
[53] H. Goto, S. Wakabayashi, M. Ikeda, M. Sakata, and K. Imanaka, "Micro focusing optical device using piezoelectric thin film actuator," in *Proceedings of SPIE - Micro-Optics/Micromechanics and Laser Scanning and Shaping*, 1995, vol. 2383, no. 8, pp. 136–143.
[54] S. Valette, "Micro-optics, a key technology in the race to microsystems," *J. Micromechanics Microengineering*, vol. 5, no. 2, pp. 74–76, 1995.
[55] V. N. Mahajan, "Ray Spot Diagrams," in *Aberration Theory Made Simple*, Bellingham, WA, USA: SPIE, 1991, pp. 56–65.

[56] W. J. Smith, "Aberrations," in *Modern optical engineering : the design of optical systems*, 3rd Ed., New York, USA: McGraw Hill, 2000, pp. 61–90.
[57] F. L. Pedrotti, L. M. Pedrotti, and L. S. Pedrotti, "Aberration Theory," in *Introduction to Optics*, 3rd Ed., Pearson Prentice Hall, 2013.
[58] M. Katz, *Introduction to Geometrical Optics*, 1st Ed. New Jersey, USA: World Scientific Publishing Company, 2002.
[59] T.-M. Wu, "Computer-aided Deflection and Slope Analyses of Beams," *J. Appl. Sci.*, vol. 6, no. 2, pp. 333–339, 2006.
[60] E. H. Thall, "Geometrical Optics," in *Duane's Ophthalmology*, 2006 Ed., Lippincott Williams and Wilkins, 2005.
[61] K. R. Spring and M. W. Davidson, "Microscope Optical Components Introduction," 2012. (Online). Available: http://www.olympusmicro.com/primer/anatomy/components.html. (Accessed: 01-Nov-2016).
[62] A. F. Ergenc, *A Novel Method for ICSI: Rotationally Oscillating Drill: Design, Control and Monitoring*. VDM Verlag, 2009.
[63] Y. Yao, Y. Hu, S. Gao, G. Yang, and J. Du, "A multipurpose dual-axis solar tracker with two tracking strategies," *Renew. Energy*, vol. 72, pp. 88–98, Dec. 2014.
[64] S. J. Oh, Y. J. Lee, K. Chen, Y. M. Kim, S. H. Lim, and W. Chun, "Development of an embedded solar tracker for the enhancement of solar energy utilization," *Int. J. Energy Res.*, vol. 36, no. 2, pp. 249–258, 2012.
[65] F. Duarte, P. D. Gaspar, and L. C. Gonçalves, "Two axis solar tracker based on solar maps , controlled by a low-power microcontroller," *Energy Power Eng.*, vol. 5, no. 7, pp. 671–676, 2011.
[66] C.-Y. Lee, P.-C. Chou, C.-M. Chiang, and C.-F. Lin, "Sun tracking systems: a review," *Sensors (Basel)*, vol. 9, no. 5, pp. 3875–90, 2009.
[67] J. M. Moreno, P. H. Magalhães, and R. Cervantes, "Inspira's CPV Sun Tracking," in *Concentrator Photovoltaics*, Berlin, Heidelberg: Springer Berlin Heidelberg, 2007, pp. 221–251.
[68] H. Mousazadeh, A. Keyhani, A. Javadi, H. Mobli, K. Abrinia, and A. Sharifi, "A review of principle and sun-tracking methods for maximizing solar systems output," *Renew. Sustain. Energy Rev.*, vol. 13, no. 8, pp. 1800–1818, Oct. 2009.
[69] F. Sallaberry, R. Pujol-Nadal, M. Larcher, and M. H. Rittmann-Frank, "Direct tracking error characterization on a single-axis solar tracker," *Energy Convers. Manag.*, vol. 105, pp. 1281–1290, 2015.
[70] M. C. Bhatnagar, J. C. Joshi, and A. K. Mukerjee, "Determination of tracking error in an automatic sun tracking system," *Sol. Wind Technol.*, vol. 4, no. 3, pp. 399–403, 1987.
[71] H. Fathabadi, "Novel high efficient offline sensorless dual-axis solar tracker for using in photovoltaic systems and solar concentrators," *Renew. Energy*, vol. 95, pp. 485–494, Sep. 2016.
[72] R. Conant, *Micromachined Mirrors*, 1st Ed. New York, USA: Springer Science+Business Media, 2003.
[73] J. A. Ogilvy, *Theory of Wave Scattering From Random Rough Surfaces*. Taylor & Francis Ltd, 1991.
[74] U. Persson, "In-process measurement of surface roughness using light scattering," *Wear*, vol. 215, no. 1–2, pp. 54–58, Mar. 1998.
[75] Layertec, "How to specify substrates," 2011. (Online). Available: https://www.layertec.de/en/capabilities/substrates. (Accessed: 06-Nov-2016).
[76] Semrock, IDEX Health & Science, and Intelligent Solutions for Life, "Practical Flatness: Tech Note," New York, USA, 2016.
[77] J. E. Harvey, S. Schröder, N. Choi, and A. Duparré, "Total integrated scatter from surfaces with arbitrary roughness, correlation widths, and incident angles," *Opt. Eng.*, vol. 51, no. 1, p. 13402, Feb. 2012.
[78] K. H. Guenther, P. G. Wierer, and J. M. Bennett, "Surface roughness measurements of low-scatter mirrors and roughness standards," *Appl. Opt.*, vol. 23, no. 21, p. 3820, 1984.
[79] H. E. Bennett and J. O. Porteus, "Relation Between Surface Roughness and Specular Reflectance at Normal Incidence," *J. Opt. Soc. Am.*, vol. 51, no. 2, p. 123, Feb. 1961.
[80] H. Davies, "The reflection of electromagnetic waves from a rough surface," *Proc. IEE - Part IV Inst. Monogr.*, vol. 101, no. 7, pp. 209–214, Aug. 1954.
[81] Engineer's Edge, "Surface Roughness Conversion Chart Tables," 2017. (Online). Available: http://www.engineersedge.com/manufacturing/surface-roughness-conversion.htm. (Accessed: 02-Mar-2017).